Journal of Science and Technology in Civil Engineering, HUCE, 2025, 19 (1): 59–71

GEOMETRICALLY NONLINEAR ANALYSIS OF FUNCTIONALLY GRADED PLATES WITH SYMMETRICAL PARABOLIC THICKNESS PROFILE UNDER UNIAXIAL COMPRESSION BASED ON ISOGEOMETRIC ANALYSIS

Thai Son[a,b,*]

[a]*Faculty of Civil Engineering, Ho Chi Minh City University of Technology (HCMUT), 268 Ly Thuong Kiet street, Ward 14, District 10, Ho Chi Minh city, Vietnam*
[b]*Vietnam National University Ho Chi Minh City (VNU-HCM), Linh Trung ward, Thu Duc city, Ho Chi Minh city, Vietnam*

Article history:
Received 02/12/2024, Revised 13/02/2025, Accepted 03/3/2025

Abstract

This paper is dedicated to the study of geometrically nonlinear behaviour of variable thickness functionally-graded plates subjected to uniaxial compressive forces. The plate's geometry in this study could have either uniform thickness or symmetrical parabolic-form thickness. To develop the theoretical formulation of the problem, the kinematics of the plates are described by the third-order shear deformation theory for plate structures with thin and moderate thickness. The geometrical nonlinearity is accounted for by von Karman's assumptions, while the rule of mixture is used to evaluate the effective material properties of functionally graded materials whose constituent phases vary across the plate's thickness. The governing equation is derived via the principle of virtual work with assumptions of small-strain problems. The Isogeometric Analysis is then used to discretize the governing equations. Arc-length iterative technique with imperfection is used to trace the equilibrium paths of the problem. Various numerical examples are also performed to validate the accuracy of the proposed numerical model and investigate the nonlinear response of the variable thickness functionally graded plates.

Keywords: functionally graded materials; geometric nonlinearity; post-buckling analysis; variable thickness; isogeometric analysis.

https://doi.org/10.31814/stce.huce2025-19(1)-06

1. Introduction

Variable-thickness plates are extensively utilized in numerous practical applications in the field of structural engineering, e.g. marine structures [1], aircraft [2], civil engineering [3], mechanical engineering [4], etc. There are various profiles of variable thickness plates that have been extensively investigated for practical applications in the literature, namely taped plates [5–7], quadratic-thickness variation plates [8, 9], and other profiles of thickness variations [10, 11]. Thanks to the preferable structural performances of variable thickness plates, there is no doubt that a large number of publications have been devoted to the analyses of the mechanical responses of variable thickness plates under different loading scenarios, e.g. static bending, free vibration, buckling and stability, etc. A recent literature review of such studies was addressed by Thai et al. [12]. Overall, the studies on mechanical behaviour of variable thickness plates conducted previously are based on analytical solutions, numerical approach, and experimental programs. Amongst those methodologies, the numerical modelling approach has been exensively adopted to the study the structural performance of variable

*Corresponding author. *E-mail address:* son.thai@hcmut.edu.vn (Son, T.)

thickness plates [12]. This fact could be attributed the complications of the problems regarding geometrical aspects and boundary conditions that are not easily treated within the framework of analytical studies.

In real-life applications, the plate-like structures are prone to extreme loading circumstances and the structures would experience large deflections. This unfavourable situation in practice necessitates the design process to account for the geometric nonlinearity of the structures to ensure a safe design. Up until now, various studies have been conducted to analyse the geometrically nonlinear response of variable thickness plates in the literature. One of the earliest studies on the nonlinear behaviour of variable thickness was carried out by Reddy and Huang [13], in which the authors employed the finite element method to study the nonlinear static bending of annular plates. By using a general finite element method, Raju and Rao [14] examined the post-buckling response of linearly tapered isotropic circular plates under thermal conditions. By using the differential quadrature method, Malekzadeh and Karami [15] studied the nonlinear flexural vibration with large amplitudes of tapered plates having elastically restrained edges. By adopting the finite element approach, Ganesan and Liu [16] present a study on the nonlinear analyses of the first-ply failure load and stability conditions of tapered laminated plates subjected to uniaxial compression. A nonlinear stability analysis of tapered curved composite plates was also conducted by Akhlaque-E-Rasul and Ganesan [17]. In this study, the authors adopted the first-ply failure analysis and the simplified non-linear buckling analysis to seek the critical properties of the tapered curved plates so that the structures would not fail before global buckling. The study of nonlinear bending and post-buckling of variable thickness plates made from isotropic and laminated composite material was presented by Le-Manh et al. [18]. In this study, the authors employed the Mindlin theory to model the kinematics of the plates and the isogeometric analysis was used to solve the problems. The nonlinear vibration and dynamic instability of internally-thickness-tapered composite plates were addressed in the study of Darabi and Ganesan [19], in which Navier's double Fourier series was employed as solution techniques and the taped plates were subjected to parametric excitation. The nonlinear bending behaviour of rectangular magnetoelectroelastic plates with linearly varying thickness was studied by Wang et al. [20], in which the differential Galerkin method was used to develop the numerical models. In the study of Dastjerdi and Tadi Beni [21], the nonlinear bending of small-scaled plates with irregular variable thickness was investigated. The plates in this study were subjected to nonuniform loading in a thermal environment, while the semi-analytical polynomial method was adopted to yield numerical solutions. A unified wavelet algorithm was proposed by Yu [22] to analyse the nonlinear static bending response of variable thickness plates, which lay on nonlinear triparametric elastic foundations. This study was also extended later to investigate the large deflection behaviour of tapered plates subjected to three-dimensionally hygrothermal stresses [23]. Recently, Thai et al. [12] studied the nonlinear bending of variable thickness plates made from multi-directional functionally graded materials based on the isogeometric analysis approach and the third-order shear deformation theory.

As highlighted in the previous literature review, previous research on the nonlinear response of variable thickness plates has not been extensively explored, especially for the geometrically nonlinear static analyses of the plate under the effects of in-plane compressive stress, i.e. post-buckling analysis [18]. Consequently, the primary objective of this study is to develop a numerical model to analyze the geometrically nonlinear response of the variable thickness plates under uniaxial compressive forces. The numerical model developed in this study could be considered as an extension of the previous work [12]. In addition, the plates addressed in this study are assumed to be made from Functionally Graded Materials (FGMs) [24] with the inhomogeneous material being graded along the thickness of

the plates. It is noted that FGMs are widely known as advanced composite materials having preferable mechanical properties compared to traditional laminated composites [25] and the investigations for the structural characteristics of plate-like structures have been extensively investigated in the literature [25–31]. To develop the governing equations of the geometrical nonlinear problems, the principle of virtual work and the third-order shear deformation theory are employed, while geometric nonlinearity is addressed using von Karman's assumptions. The Isogeometric Analysis (IGA) approach, recognized as an advanced finite element method [32, 33], is used to discretize the governing equation to establish the system equation of the problems. To deal with the nonlinear algebraic system equation, the acr-length iterative technique with imperfection is adopted. Various numerical examples are also presented to validate the accuracy of the proposed numerical model and analyse the geometrically nonlinear behaviour of the variable thickness functionally graded (FG) plates.

2. Mathematical formulation

2.1. Profile of variable thickness plates and material homogenisation

In this study, rectangular plates having a uniform thickness (denoted UT plates) and symmetrical parabolic-form thickness (denoted as PT plates) are investigated. The geometrical profiles and origin or Cartesian coordinates are depicted in Fig. 1. It is assumed that the PT plates only have variable thickness along the x-direction and the thickness profile is symmetrical to the middle plane of the plates.

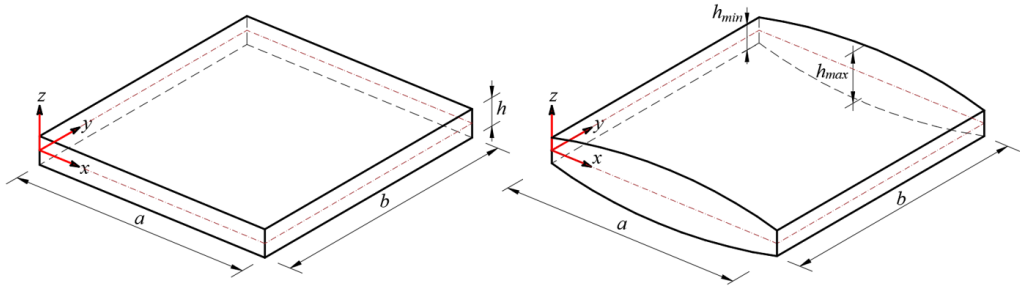

Figure 1. Geometrical profiles of uniform-thickness plate (left) and symmetrical parabolic-form thickness plate (right)

Mathematical expression of the thickness profile of the plates is given by:

$$z_t(x,y) = -z_b(x,y) = \frac{h_{\min}}{2} + 2\left(h_{\max} - h_{\min}\right)\left\{\frac{x}{a} - \left(\frac{x}{a}\right)^2\right\} \tag{1}$$

where z_t and z_b are the coordinates along the z-axis of the top surface and bottom surface, respectively, $h_{\min}$ and $h_{\max}$ are the smallest and largest thickness of the plate along the x-direction. The planar sizes of the rectangular plates are a and b as shown in Fig. 1. As the coordinate origin is located in the middle plane of the plate, the uniform-thickness profile can be obtained by setting $h_{\min} = h_{\max}$ and the thickness of the plate is given by: $h\,(x,y) = z_t(x,y) - z_b(x,y)$.

Both UT plates and PT plates addressed in this study are assumed to be made from FGMs whose material constituents are graded long thickness direction. By adopting the rule of mixture [34], effective elastic modulus E_e and effective Poisson's ration ν_e are given by

$$E_e = \left(E_c - E_m\right)V_c + E_m; \quad \nu_e = \left(\nu_c - \nu_m\right)V_c + \nu_m \tag{2}$$

where subscripts c and m denote the material properties of ceramic and metal phases, respectively. V_c represent the volume fraction of the ceramic constituent is given by

$$V_c = \left(\frac{z}{h} + \frac{1}{2}\right)^n \tag{3}$$

in which n is the material gradient index. As seen in Eqs. (2) and (3), the material variation profiles at every location within the PT plate are similar as given in Eq. (3), however, the actual volumes of material phases are different due to the variation of plate thickness $h(x, y)$ along planar directions.

2.2. Kinematics and governing equation of the geometrically nonlinear problems

To describe the kinematics of the plates, the equivalent single-layer model based on the third-order shear deformation plate theory proposed by Reddy [35] is employed:

$$\left\{\begin{array}{c} u_1 \\ u_2 \\ u_3 \end{array}\right\} = \left\{\begin{array}{c} u \\ v \\ w \end{array}\right\} + f(z)\left\{\begin{array}{c} \theta_x \\ \theta_y \\ 0 \end{array}\right\} + g(z)\left\{\begin{array}{c} -w_{,x} \\ -w_{,y} \\ 0 \end{array}\right\} \tag{4}$$

where $f(z) = z - 4z^3/3h^2; g(z) = 4z^3/3h^2$; u_1, u_2, and u_3 are displacements of any material point within the plate's domain along x, y, and z directions, respectively; u, v, and w are corresponding displacements of material points location on the middle plane of the plates; θ_x and θ_y are the corresponding rotations along x and y directions, the comma notation denotes the partial derivative.

The nonlinear strain-displacement relations in the sense of von Karman's assumptions are presented by

$$\varepsilon = \varepsilon_0 + f(z)\,\varepsilon_1 + g(z)\,\varepsilon_2 + \frac{1}{2}\varepsilon_{nl}; \quad \gamma = f'(z)\,\gamma_1 + (1 - g'(z))\,\gamma_2 \tag{5}$$

in which the prime notation represents the derivative with respect to z, and

$$\varepsilon = \left\{\begin{array}{c} \varepsilon_{xx} \\ \varepsilon_{yy} \\ \gamma_{xy} \end{array}\right\}; \varepsilon_0 = \left\{\begin{array}{c} u_{,x} \\ v_{,y} \\ u_{,y} + v_{,x} \end{array}\right\}; \varepsilon_1 = \left\{\begin{array}{c} \theta_{x,x} \\ \theta_{y,y} \\ \theta_{x,y} + \theta_{y,x} \end{array}\right\}; \varepsilon_2 = \left\{\begin{array}{c} -w_{,xx} \\ -w_{,yy} \\ -2w_{,xy} \end{array}\right\}; \varepsilon_{nl} = \left\{\begin{array}{c} (w_{,x})^2 \\ (w_{,y})^2 \\ 2w_{,x}w_{,y} \end{array}\right\} \tag{6}$$

$$\gamma = \left\{\begin{array}{c} \gamma_{xz} \\ \gamma_{yz} \end{array}\right\}; \quad \gamma_1 = \left\{\begin{array}{c} \theta_x \\ \theta_y \end{array}\right\}; \quad \gamma_2 = \left\{\begin{array}{c} w_{,x} \\ w_{,y} \end{array}\right\} \tag{7}$$

According to the von Karman's assumptions [36, 37], nonlinear strains and stress resultants are derived by assuming that the rotational in terms of transverse displacement can be moderate and their squares and products can not be neglected. This means that all the nonlinear components in the Green Largrange strains can be neglected except those related to the derivatives of transverse displacements in the plate problems. The von Karman's assumption has been extensively used in the literature to analyse the geometrical nonlinear response of plate structures and physically accurate results can be obtained for the plates that undergo large displacements yet moderate rotations [38].

For plate problems, the constitutive equation is given in Eq. (8), in which the stretching of the plates along the thickness direction and corresponding stress component is neglected.

$$\left\{\begin{array}{c} \sigma_{xx} \\ \sigma_{yy} \\ \sigma_{xy} \end{array}\right\} = \mathbf{Q}_b \left\{\begin{array}{c} \varepsilon_{xx} \\ \varepsilon_{yy} \\ \gamma_{xy} \end{array}\right\}; \quad \left\{\begin{array}{c} \sigma_{xz} \\ \sigma_{yz} \end{array}\right\} = \mathbf{Q}_s \left\{\begin{array}{c} \gamma_{xz} \\ \gamma_{yz} \end{array}\right\} \tag{8}$$

$$\mathbf{Q}_b = \frac{E_e}{1 - \nu_e^2}\begin{bmatrix} 1 & \nu_e & 0 \\ \nu_e & 1 & 0 \\ 0 & 0 & (1 - \nu_e)/2 \end{bmatrix}; \quad \mathbf{Q}_s = \frac{E_e}{(1 + \nu_e)}\begin{bmatrix} 1 & 0 \\ 0 & 1 \end{bmatrix} \tag{9}$$

The governing equation of the geometrically nonlinear problems of the plates under uniaxial compression is derived by using the principle of virtual. In addition, small-strain assumptions, especially for plate problems, are adopted such that there could be no differences between stress and strain measures [37]. Therefore, the governing equation can be presented in accordance with the initial undeformed geometry as follows

$$\int_V \sigma_{ij}\delta\varepsilon_{ij}dV = \int_S t_i\delta u_i dS \tag{10}$$

where V denotes the volume of the plates, S presents the boundaries where the compressive forces are applied, t_i is the compressive force and u_i is the associated degree of freedom to which the load is applied.

By substituting Eqs. (5) and (8) into Eq. (10), and take integration over the thickness h, the governing equation can be rewritten as follows

$$\int_\Omega \delta\left(\bar{\boldsymbol{\varepsilon}} + \frac{1}{2}\bar{\boldsymbol{\varepsilon}}_{nl}\right)^T \bar{\mathbf{C}}\left(\bar{\boldsymbol{\varepsilon}} + \frac{1}{2}\bar{\boldsymbol{\varepsilon}}_{nl}\right) d\Omega = \int_S \delta\bar{\mathbf{u}}^T\bar{\mathbf{t}}dS \tag{11}$$

where Ω designates the middle plane of the plate as an equivalent single-layer model. Other components in Eq. (11) can be presented by:

$$\bar{\boldsymbol{\varepsilon}} = \begin{Bmatrix} \boldsymbol{\varepsilon}_0 \\ \boldsymbol{\varepsilon}_1 \\ \boldsymbol{\varepsilon}_2 \\ \boldsymbol{\gamma}_1 \\ \boldsymbol{\gamma}_2 \end{Bmatrix}; \quad \bar{\boldsymbol{\varepsilon}}_{nl} = \begin{Bmatrix} \boldsymbol{\varepsilon}_{nl} \\ \mathbf{0} \\ \mathbf{0} \\ \mathbf{0} \\ \mathbf{0} \end{Bmatrix} \tag{12}$$

$$\bar{\mathbf{C}} = \begin{bmatrix} \mathbf{C}_{b11} & \mathbf{C}_{b12} & \mathbf{C}_{b13} & \mathbf{0} & \mathbf{0} \\ \mathbf{C}_{b12} & \mathbf{C}_{b22} & \mathbf{C}_{b23} & \mathbf{0} & \mathbf{0} \\ \mathbf{C}_{b13} & \mathbf{C}_{b23} & \mathbf{C}_{b33} & \mathbf{0} & \mathbf{0} \\ \mathbf{0} & \mathbf{0} & \mathbf{0} & \mathbf{C}_{s11} & \mathbf{C}_{s12} \\ \mathbf{0} & \mathbf{0} & \mathbf{0} & \mathbf{C}_{s12} & \mathbf{C}_{s22} \end{bmatrix} \tag{13}$$

$$\begin{aligned} (\mathbf{C}_{b11}, \mathbf{C}_{b12}, \mathbf{C}_{b13}) &= \int_{z_b}^{z_t} (1, f(z), g(z))\,\mathbf{Q}_b dz \\ (\mathbf{C}_{b22}, \mathbf{C}_{b23}, \mathbf{C}_{b33}) &= \int_{z_b}^{z_t} \left((f(z))^2, f(z)\,g(z), (g(z))^2\right)\mathbf{Q}_b dz \\ (\mathbf{C}_{s11}, \mathbf{C}_{s12}, \mathbf{C}_{s22}) &= \int_{z_b}^{z_t} \left((f'(z))^2, (f'(z))(1-g'(z)), (1-g'(z))^2\right)\mathbf{Q}_s dz \end{aligned} \tag{14}$$

It is noted that $\mathbf{C}_{b12}$ and $\mathbf{C}_{b13}$ are zero matrices once the plates are homogeneous, i.e. the neutral surface and the mid-plane are identical. For the plates with nonhomogeneous material in the thickness direction like FG plates in this study, these matrices include non-zero components due to the differences between the neutral surface and middle plane. The appearance of such components leads to a coupling relation between membrane stress resultants and bending stress resultants in the governing equation. For problems with only inplane forces being considered, the components of $\bar{\mathbf{u}}$ and $\bar{\mathbf{t}}$ are given by:

$$\begin{Bmatrix} u & v \end{Bmatrix}^T; \quad \bar{\mathbf{t}} = \begin{Bmatrix} t_x & t_y \end{Bmatrix}^T \tag{15}$$

2.3. NURBS-based discretization and solution methodology

In this section, the governing equation obtained previously is discretized by using the IGA approach, whereby NURBS basis functions are used to present the geometry of the plates and serve as interpolation functions of displacement variables:

$$\mathbf{S}_{1D}(\xi) = \sum_{i=1}^{n} \mathbf{P}_i N_i^p(\xi) \tag{16}$$

$$\mathbf{\Omega}_{2D} = \sum_{i=1}^{n}\sum_{j=1}^{m} R_{i,j}^{p,q}(\xi,\eta)\mathbf{B}_{i,j} \tag{17}$$

$$\mathbf{u} = \sum_{i=1}^{ncp} R_i(\xi,\mu)\mathbf{d}_i \tag{18}$$

$$\mathbf{u} = \left\{ \begin{array}{ccccc} u & v & \theta_x & \theta_y & w \end{array} \right\}^T; \quad \mathbf{d}_i = \left\{ \begin{array}{ccccc} u_i & v_i & \theta_{xi} & \theta_{yi} & w_i \end{array} \right\}^T \tag{19}$$

where $\mathbf{P}$ and $\mathbf{B}$ are the set of control nets used to define the geometry of the plates' boundaries and the middle plane of the plates, $\mathbf{d}$ is the displacement-variable vector associated with a control point, n and m denote the indices of control points within the control net, while ncp is the total number of control points used to define an element. $N(\xi)$ and $R(\xi, \eta)$ are 1D and 2D NURBS basic functions. Detailed expressions about NURBS functions and IGA are skipped in this section since the approach has been employed extensively for beams, plates, shells, and other structural mechanics problems [39]. The fundamentals of NURBS and IGA can be found in the monograph book [33] and the original study [32].

Based on the IGA approach with NURBS being used as interpolation functions, the following system equation is obtained from the governing equation given in Eq. (11):

$$\mathbf{K}\mathbf{d} = \mathbf{F} \tag{20}$$

in which

$$\mathbf{K} = \int_{\Omega} \left(\bar{\mathbf{B}}_{lT}^T \bar{\mathbf{C}} \bar{\mathbf{B}}_l + \frac{1}{2}\bar{\mathbf{B}}_{lT}^T \bar{\mathbf{C}} \bar{\mathbf{B}}_{nl} + \bar{\mathbf{B}}_{nlT}^T \bar{\mathbf{C}} \bar{\mathbf{B}}_l + \frac{1}{2}\bar{\mathbf{B}}_{nlT}^T \bar{\mathbf{C}} \bar{\mathbf{B}}_{nl} \right) d\Omega \tag{21}$$

$$\mathbf{F} = \int_{S} \mathbf{N}_S^T \hat{\mathbf{t}} dS \tag{22}$$

$$\bar{\mathbf{B}}_l = \left\{ \begin{array}{c} \mathbf{B}_{\varepsilon 0} \\ \mathbf{B}_{\varepsilon 1} \\ \mathbf{B}_{\varepsilon 2} \\ \mathbf{B}_{\gamma 1} \\ \mathbf{B}_{\gamma 2} \end{array} \right\}; \quad \bar{\mathbf{B}}_{lT} = \left\{ \begin{array}{c} \mathbf{B}_{\varepsilon 0}^T \\ \mathbf{B}_{\varepsilon 1}^T \\ \mathbf{B}_{\varepsilon 2}^T \\ \mathbf{B}_{\gamma 1}^T \\ \mathbf{B}_{\gamma 2}^T \end{array} \right\}; \quad \bar{\mathbf{B}}_{nl} = \left\{ \begin{array}{c} \mathbf{B}_{\varepsilon nl} \\ \mathbf{0} \\ \mathbf{0} \\ \mathbf{0} \\ \mathbf{0} \end{array} \right\}; \quad \bar{\mathbf{B}}_{nlT} = \left\{ \begin{array}{c} \mathbf{B}_{\varepsilon nl}^T \\ \mathbf{0} \\ \mathbf{0} \\ \mathbf{0} \\ \mathbf{0} \end{array} \right\} \tag{23}$$

$$\mathbf{N}_S = \left\{ \begin{array}{ccccc} N_s(\xi) & N_s(\xi) & 0 & 0 & 0 \end{array} \right\}; \quad \hat{\mathbf{t}} = \left\{ \begin{array}{ccccc} t_x & t_y & 0 & 0 & 0 \end{array} \right\} \tag{24}$$

where $\mathbf{B}_{\varepsilon 0}$, $\mathbf{B}_{\varepsilon 1}$, $\mathbf{B}_{\varepsilon 2}$, $\mathbf{B}_{\gamma 1}$, $\mathbf{B}_{\gamma 2}$, and $\mathbf{B}_{\varepsilon nl}$ are strain-displacement matrices, whose details are given as follows:

$$\varepsilon_0 = \mathbf{B}_{\varepsilon 0}\mathbf{d}; \quad \varepsilon_1 = \mathbf{B}_{\varepsilon 1}\mathbf{d}; \quad \varepsilon_2 = \mathbf{B}_{\varepsilon 2}\mathbf{d}; \quad \gamma_1 = \mathbf{B}_{\gamma 1}\mathbf{d}; \quad \gamma_2 = \mathbf{B}_{\gamma 2}\mathbf{d}; \quad \varepsilon_{nl} = \mathbf{B}_{\varepsilon nl}\mathbf{d} \tag{25}$$

$$\mathbf{B}_{\varepsilon 0} = \begin{bmatrix} R_{,x} & 0 & 0 & 0 & 0 \\ 0 & R_{,y} & 0 & 0 & 0 \\ R_{,y} & R_{,x} & 0 & 0 & 0 \end{bmatrix}; \quad \mathbf{B}_{\varepsilon 1} = \begin{bmatrix} 0 & 0 & R_{,x} & 0 & 0 \\ 0 & 0 & 0 & R_{,y} & 0 \\ 0 & 0 & R_{,y} & R_{,x} & 0 \end{bmatrix} \tag{26}$$

$$\mathbf{B}_{\varepsilon 2} = \begin{bmatrix} 0 & 0 & 0 & 0 & -R_{,xx} \\ 0 & 0 & 0 & 0 & -R_{,yy} \\ 0 & 0 & 0 & 0 & -2R_{,xy} \end{bmatrix}; \quad \mathbf{B}_{\gamma 1} = \begin{bmatrix} 0 & 0 & R_c & 0 & 0 \\ 0 & 0 & 0 & R_c & 0 \end{bmatrix}; \quad \mathbf{B}_{\gamma 2} = \begin{bmatrix} 0 & 0 & 0 & 0 & R_{,x} \\ 0 & 0 & 0 & 0 & R_{,y} \end{bmatrix} \tag{27}$$

It is noted that the C^1-continuity requirement in developing those matrices is satisfied naturally based on the inherent features of the IGA approach.

To solve the nonlinear equation presented in Eq. (20) for plate structures subjected to in-plane compressive forces, the arc-length technique is used in this study. It is worth noting that the adoption of the arc-length technique in this study aims to generalize the numerical model, enabling it to trace potential stability paths of the plates under in-plane compressive forces, such as snap-through and snap-back paths. Detailed procedure of the arc-length technique could be found in the well-known textbooks of Crisfield [40] and Reddy [37]. The iterative numerical technique requires the development of a tangent stiffness matrix, which is given as follows [12]:

$$\mathbf{K}_T = \frac{\partial \mathbf{K}}{\partial \mathbf{d}}\mathbf{d} + \mathbf{K} = \int_\Omega \left(\bar{\mathbf{B}}_{lT}^T \bar{\mathbf{C}} \bar{\mathbf{B}}_l + \bar{\mathbf{B}}_{lT}^T \bar{\mathbf{C}} \bar{\mathbf{B}}_{nl} + \bar{\mathbf{B}}_{nlT}^T \bar{\mathbf{C}} \bar{\mathbf{B}}_l + \bar{\mathbf{B}}_{nlT}^T \bar{\mathbf{C}} \bar{\mathbf{B}}_{nl} + \bar{\mathbf{B}}_g^T \bar{\mathbf{N}} \bar{\mathbf{B}}_g \right) d\Omega \tag{28}$$

in which

$$\mathbf{B}_g = \begin{bmatrix} 0 & 0 & 0 & 0 & R_{,x} \\ 0 & 0 & 0 & 0 & R_{,y} \end{bmatrix} \tag{29}$$

$$\bar{\mathbf{N}} = \begin{bmatrix} N_x & N_{xy} \\ N_{xy} & N_y \end{bmatrix} \tag{30}$$

$$\begin{Bmatrix} N_x \\ N_y \\ N_{xy} \end{Bmatrix} = \mathbf{C}_{b11} \left(\varepsilon_0 + \frac{1}{2}\varepsilon_{nl} \right) + \mathbf{C}_{b11}\varepsilon_1 + \mathbf{C}_{b13}\varepsilon_2 \tag{31}$$

To alleviate the numerical difficulties in solving the nonlinear problems of plate structures subjected to in-plane compressive forces, a relatively small imperfection is imposed on the initial geometry of the plates [41]. In this study, the imperfection profile of rectangular plates is assumed to have a sinusoidal shape, and only transverse deflections are considered as given by

$$w_{imf} = w_0 \sin\left(\frac{\pi x}{a}\right) \sin\left(\frac{\pi y}{b}\right) \tag{32}$$

where w_0 is the magnitude of the imperfection and it is taken as $0.001h_{\min}$. After conducting numerical tests, this imperfection value is shown to be sufficient for yielding stable equilibrium paths without affecting the overall response of the structures.

3. Numerical examples

3.1. Verification examples

In this section, the accuracy of the proposed numerical model is assessed by revisiting the previous post-buckling problems studied previously in the literature. The first verification example is dedicated to the post-buckling problem of a rectangular FG plate having a uniform thickness, which was investigated by Sitli et al. [42]. The FG plate in this example has planar dimensions of $a =$

0.25 m, $b = 0.5$ m, and the thickness ratio is $h/b = 0.01$. The plate is subjected to a uniformly distributed compressive force N_x at $x = 0$ and $x = a$. The ceramic and metal constituents of the plates are Al_2O_3 and Al, respectively, with $E_c = 380$ GPa, $E_m = 70$ GPa, $\nu_c = \nu_m = 0.3$, and $n = 1$. Two types of boundary conditions are investigated in this example, namely simply supported *SSSS* and clamped *CCCC*. Details of those boundary conditions are given as follows:

$$SSSS: \begin{cases} w = \theta_y = 0 & \text{at } x = 0, a \\ w = \theta_x = 0 & \text{at } y = 0, b \end{cases}; \quad CCCC: \begin{cases} w = \theta_x = \theta_y = w_{,x} = 0 & \text{at } x = 0, a \\ w = \theta_x = \theta_y = w_{,y} = 0 & \text{at } y = 0, b \end{cases} \tag{33}$$

In Fig. 2, comparisons between the post-buckling paths obtained from Sitli et al. [42] and those obtained from the present study are illustrated. In general, a good agreement between numerical results presented from the proposed numerical model and those from the referenced results is archived. However, the numerical results obtained from the present study are slightly different from referenced results for the *CCCC* plates. Such differences could be attributed to the fact that Sitli et al. [42] only used the classical plate theory to describe the kinematics of the plates. Therefore, the shear deformation effect, which is expected to be considerable in clamped plates rather than simply supported plates, is dismissed. Regarding the mesh size, it is noted that a mesh size of 14×14 with cubic NURBS basis functions is used to produce all numerical results of this study. This mesh size is shown to be fine enough to get the converged results in the convergence study, which is not presented herein for the sake of brief.

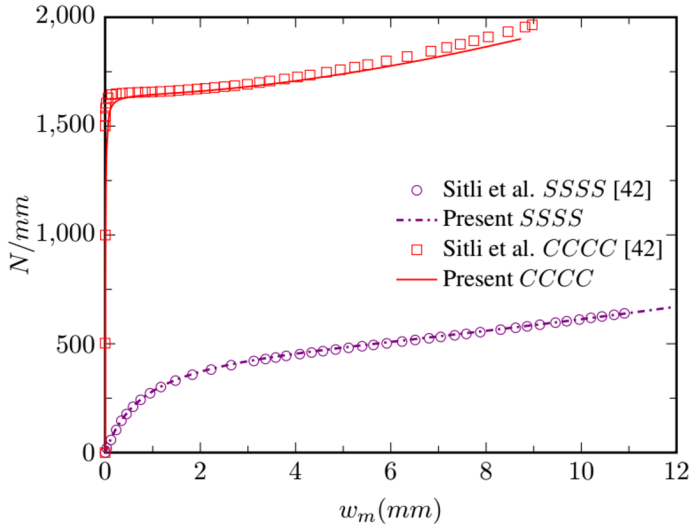

Figure 2. Comparisons between post-buckling paths of rectangular FG plates with uniform thickness ($a/b = 0.5$, $a = 250$ mm, $h/b = 0.01$, w_m is the transverse displacement at the center of the plate)

The next verification example is about the post-buckling response of isotropic square plate having sine-wave thickness along the x direction [18]. The thickness profile of the plate is given by

$$z_t(X) = -z_b(X) = \alpha\bar{h}\sin\left(2\pi\frac{nX}{a} + \frac{\pi}{2}\right) + \frac{\bar{h}}{2}; \quad X = x - \frac{a}{2} \tag{34}$$

where $\alpha = 0.1$ and $n = 2$. The square plate has a side length of $a = 10$ m and $\bar{h}$= 0.5 m. Material properties of the plate are $E = 3{\times}10^6$ N/m^2 and $\nu = 0.25$. The plate is simply supported (*SSSS*) and is subjected to uniform axial compressive forces N_y along y direction. Comparisons between the

referenced equilibrium path and one obtained from the present study is depicted in Fig. 3. Herein $\lambda = Na^2/\pi^2\bar{D}, \bar{D} = E\bar{h}^3/12\left(1-\nu^2\right)$, $\lambda_{ycr}^{\alpha=0} = 3.4636$ is the critical buckling load of the referenced uniform thickness plate, and w_m is the transverse displacement at the center of the plate. Overall, the numerical results obtained from this study agree well with those produced previously by Le-Manh et al. [18].

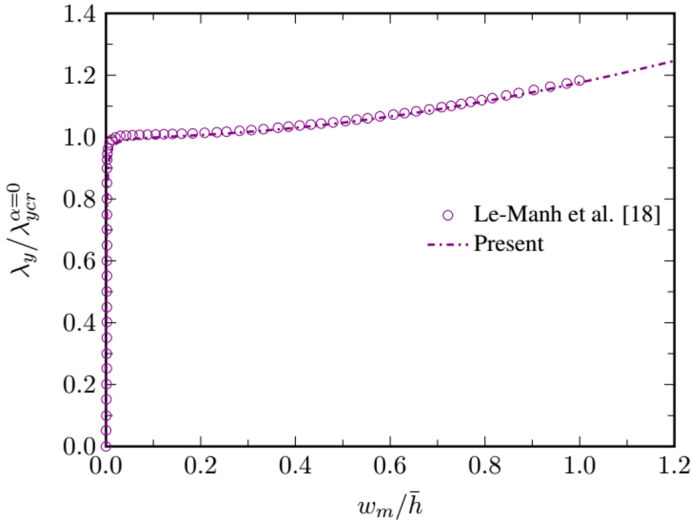

Figure 3. Comparison of post-buckling paths of an isotropic square plate having sine-wave thickness along x direction under compressive force along the y direction

3.2. Parametric studies

In this section, some numerical examples are presented to study the post-buckling behaviour of FG plates with symmetrical parabolic-form thickness profile (PT) being shown in Section 2.1. The plates examined herein are square with a side length of $a = 1$ m and the value of $h_{\min}$ is fixed with $h_{\min} = a/20$. Similar to the first verification example, the plates are assumed to be made from Al_2O_3 (ceramic) and Al (metal) constituents: $E_c = 380$ GPa, $E_m = 70$ GPa, $\nu_c = \nu_m = 0.3$. The following nondimensional compressive load is used subsequently

$$\bar{N}_x = b^2 N_x \Big/ E_m h_{\min}^3 \tag{35}$$

The first parametric study is about the influence of material gradation on the nonlinear response of uniform thickness plate (UT plate model, $h = h_{\min} = a/20$) and variable thickness (PT plate model, $h_{\min} = a/20$, $h_{\max} = 1.1h_{\min}$). The plates are simply supported (*SSSS* boundary condition) and subject to uniform compressive forces along the x direction. By changing the value of the gradient index n, different material gradations could be obtained. As shown in Fig. 4, the increase of gradient index n reduces the strength of the plates. It is noted that the notations Al_{203} and Al in the figure represent the cases where material within the plate is homogeneous with fully ceramic and fully metal, respectively. The reduction in the strength of the plate is understandable as the elevation of the gradient index leads to a decrease in the stiffness of the plate as more metal constituents appear within the plate's volume.

Another important point that should be pointed out is the trends of post-buckling paths. For uniform thickness plate (UT plate), the nonlinear responses of homogeneous plates are bifurcation buckling, where sudden changes in deformation pattern are observed when the compressive forces increase to the values close to the critical buckling loads. For FG plates with uniform thickness,

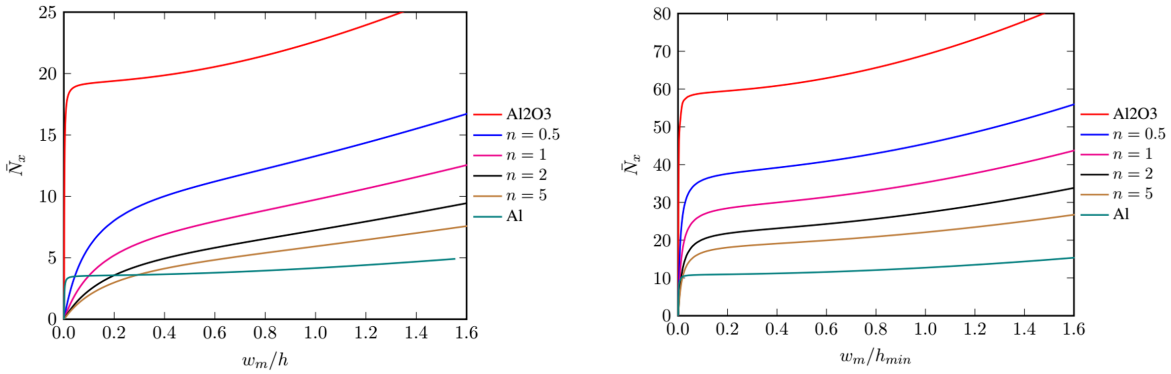

(a) Uniform-thickness plates (UT)

(b) Variable thickness plate (PT $h_{\max} = 1.1h_{\min}$)

Figure 4. Post-buckling response of simply-supported FG plates under uniform compressive forces

i.g. inhomogeneous along the thickness direction, the plates deform immediately when the loads are applied to the structures, consequently, the deflections of the plates increase gradually. This phenomenon can be explained by the actual difference between the neutral plane and the middle plane of the plate, where the inplane compressive forces are imposed. Such difference induces a coupling bending moment and makes the plate bend in the upward direction. For the plates with variable thickness (PT plate), bifurcation post-buckling paths are also obtained in cases of homogeneous plates (Al_2O_3 and Al). However, the equilibrium paths of FG plates (inhomogeneous cases) are somewhat close to the bifurcation response, although the changes in the deformation paths are not as abrupt as those seen in the bifurcation responses. In this case, the neutral axis of each section of the plate alters gradually due to the change in the plate thickness. This physical aspect might lead to a non-uniform coupling bending moment along the planar direction of the plates, and hence the effect of the coupling moment is not as significant as those observed in uniform thickness plates.

In the second investigation in this section, the effects of plates' thickness profiles and boundary conditions are addressed. The post-buckling paths of the plates with different thickness profiles (by changing the ratio of $h_{\max}/h_{\min}$) and boundary conditions are shown in Fig. 5. The planar dimensions, minimum thickness ($h_{\min}$), and material properties of the plates are identical to the previous example. The plate is also subjected to uniform compressive load along the x-direction only and the material constituents are graded along the thickness direction with $n = 2$. As illustrated in Fig. 5, two noticeable observations should be pointed out. Firstly, the equilibrium paths of uniform thickness plate (UT plate model with $h_{\max}/h_{\min} = 1.0$) are completely different for inhomogeneous plates with simply supported boundary condition (*SSSS*) and clamped boundary condition (*CCCC*). While the bifurcation response is observed in the case of the clamped plate with uniform thickness, the simply supported plate deforms progressively with the increase of the imposed compressive load. As discussed earlier, the coupling bending moment induced by the difference between the neutral surface and middle plane makes the plate deform in the transverse direction. For the uniform thickness plate with clamped boundary conditions, the restraints of rotations along the boundaries could be the major factor preventing the early deforms of the plates, therefore, bifurcation buckling exists.

The second interesting observation shown in Fig. 5 is the similar trends of the equilibrium paths of variable thickness plates. It is seen that the responses of simply supported plates and clamped plates with symmetrical parabolic-form thickness are almost identical. In addition, no bifurcation buckling path is captured. These results indicate that the effects of clamped boundary conditions

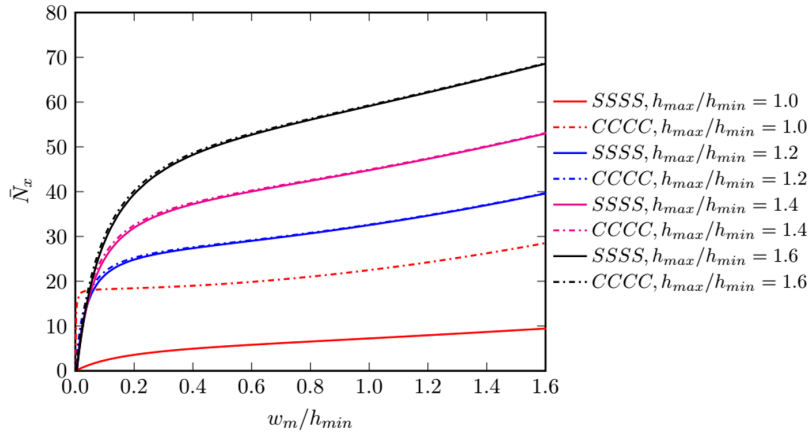

Figure 5. Comparisons of the post-buckling paths of FG plates (n = 2) with different thickness profiles and boundary conditions

become insignificant for the PT thickness profile addressed in this study. As the thickness of the plate is smaller at the boundaries (where the compressive forces are applied) and becomes larger at the center region, the coupling bending moment at the center region is larger than those around the boundaries and the capacity to present early deformations (transverse deflections cause rotations at regions near the boundaries) is reduced. Therefore, those plates deform gradually with the increase of compressive forces.

4. Conclusions

In this study, the geometrically nonlinear behaviour of variable thickness FG plates under uniaxial compressive forces is investigated. The governing equation of the nonlinear problem is developed by the principle of virtual work, in which the third-order shear deformation theory is used to describe the displacement field of the plates and von Karman assumptions are used to capture the geometrical nonlinear effects. By adopting the IGA approach, the system equation is developed and the arc-length iterative technique with imperfection is used to solve the nonlinear system equation. After verifying the accuracy of the proposed numerical model, parametric investigations are conducted. From the numerical results, two noticeable conclusions are drawn: (i) The trends in the nonlinear response of FG plates with symmetrical parabolic-form thickness are different from those observed from uniform-thickness FG plates with inhomogeneous material along the thickness direction. The deformations of variable thickness plates are shown to be less influenced by the coupling bending moment, however, the deformation rate is not as pronounced as that observed in the bifurcation buckling response. (ii) The influence of clamped boundary conditions is not considerable for plates with larger thicknesses at their center region and the responses are almost identical the the simply supported plates. In future work, the numerical developed in this study could be further developed to deal with the post-buckling analysis of plates having more complicated thickness profiles. Different mechanical loading patterns, materials, and thermal loads could be also investigated from the numerical model presented in this study.

Acknowledgements

This research is funded by Ho Chi Minh City University of Technology – VNU-HCM, under grant number To-KTXD-2024-19. The author acknowledges Ho Chi Minh City University of Technology (HCMUT), VNU-HCM for supporting this study.

References

[1] Datta, N., Jindal, R. (2019). Modelling a spade rudder as a hollow two-way tapered Kirchhoff's plate: Free dry and wet vibration study with numerical verification. *Applied Ocean Research*, 82:385–396.

[2] Ahari, M. N., Eshghi, S., Ashtiany, M. G. (2009). The tapered beam model for bottom plate uplift analysis of unanchored cylindrical steel storage tanks. *Engineering Structures*, 31(3):623–632.

[3] Susantha, K. A. S., Aoki, T., Kumano, T. (2006). Strength and ductility evaluation of steel bridge piers with linearly tapered plates. *Journal of Constructional Steel Research*, 62(9):906–916.

[4] Bowyer, E. P., O'Boy, D. J., Krylov, V. V., Gautier, F. (2013). Experimental investigation of damping flexural vibrations in plates containing tapered indentations of power-law profile. *Applied Acoustics*, 74 (4):553–560.

[5] Bedynek, A., Real, E., Mirambell, E. (2013). Tapered plate girders under shear: Tests and numerical research. *Engineering Structures*, 46:350–358.

[6] Lotfi, S., Azhari, M., Heidarpour, A. (2011). Inelastic initial local buckling of skew thin thickness-tapered plates with and without intermediate supports using the isoparametric spline finite strip method. *Thin-Walled Structures*, 49(11):1475–1482.

[7] Rajagopal, A., Hodges, D. H. (2015). Variational asymptotic analysis for plates of variable thickness. *International Journal of Solids and Structures*, 75-76:81–87.

[8] Zenkour, A. M. (2003). An exact solution for the bending of thin rectangular plates with uniform, linear, and quadratic thickness variations. *International Journal of Mechanical Sciences*, 45(2):295–315.

[9] Xu, Y., Zhou, D., Liu, K. (2010). Three-Dimensional Thermoelastic Analysis of Rectangular Plates with Variable Thickness Subjected to Thermomechanical Loads. *Journal of Thermal Stresses*, 33(12): 1136–1155.

[10] Shufrin, I., Eisenberger, M. (2006). Vibration of shear deformable plates with variable thickness—First-order and higher-order analyses. *Journal of Sound and Vibration*, 290(1):465–489.

[11] Bacciocchi, M., Eisenberger, M., Fantuzzi, N., Tornabene, F., Viola, E. (2016). Vibration analysis of variable thickness plates and shells by the Generalized Differential Quadrature method. *Composite Structures*, 156:218–237.

[12] Thai, S., Do, D. T. T., Tan, T. N. (2022). Nonlinear bending analysis of variable thickness multi-directional functionally graded plates based on isogeometric analysis. *Mechanics of Advanced Materials and Structures*, 30(20):4091–4109.

[13] Reddy, J. N., Haung, C. L. (1981). Nonlinear axisymmetric bending of annular plates with varying thickness. *International Journal of Solids and Structures*, 17(8):811–825.

[14] Raju, K. K., Rao, G. V. (1996). Thermal post-buckling of linearly tapered moderately thick isotropic circular plates. *Computers & Structures*, 58(3):655–658.

[15] Malekzadeh, P., Karami, G. (2008). Large amplitude flexural vibration analysis of tapered plates with edges elastically restrained against rotation using DQM. *Engineering Structures*, 30(10):2850–2858.

[16] Ganesan, R., Liu, D. Y. (2008). Progressive failure and post-buckling response of tapered composite plates under uni-axial compression. *Composite Structures*, 82(2):159–176.

[17] Akhlaque-E-Rasul, S., Ganesan, R. (2012). Non-linear buckling analysis of tapered curved composite plates based on a simplified methodology. *Composites Part B: Engineering*, 43(2):797–804.

[18] Le-Manh, T., Huynh-Van, Q., Phan, T. D., Phan, H. D., Nguyen-Xuan, H. (2017). Isogeometric nonlinear bending and buckling analysis of variable-thickness composite plate structures. *Composite Structures*, 159:818–826.

[19] Darabi, M., Ganesan, R. (2017). Non-linear vibration and dynamic instability of internally-thickness-tapered composite plates under parametric excitation. *Composite Structures*, 176:82–104.

[20] Wang, F., Zheng, Y., Chen, C. (2018). Nonlinear Bending of Rectangular Magnetoelectroelastic Thin Plates with Linearly Varying Thickness. *International Journal of Nonlinear Sciences and Numerical Simulation*, 19(3–4):351–356.

[21] Dastjerdi, S., Tadi Beni, Y. (2019). A novel approach for nonlinear bending response of macro- and nanoplates with irregular variable thickness under nonuniform loading in thermal environment. *Mechanics Based Design of Structures and Machines*, 47(4):453–478.

[22] Yu, Q. (2020). Wavelet-based homotopy method for analysis of nonlinear bending of variable-thickness plate on elastic foundations. *Thin-Walled Structures*, 157:107105.
[23] Yu, Q. (2021). Large deflection bending analysis of variable-thickness tapered plates under three-dimensionally hygrothermomechanical loads. *International Journal of Mechanical Sciences*, 207:106648.
[24] Koizumi, M. (1993). The concept of FGM. *Ceramic Transactions, Functionally Gradient Materials*, 34: 3–10.
[25] Thai, H.-T., Kim, S.-E. (2015). A review of theories for the modeling and analysis of functionally graded plates and shells. *Composite Structures*, 128:70–86.
[26] Thai, S., Lieu X., Q. (2022). Investigate the bending and free vibration responses of multi-directional functionally graded plates with variable thickness based on isogeometric analysis. *Journal of Science and Technology in Civil Engineering (JSTCE) - HUCE*, 16(4):10–29.
[27] Dinh Duc, N., Hong Cong, P. (2014). Nonlinear postbuckling of an eccentrically stiffened thin FGM plate resting on elastic foundations in thermal environments. *Thin-Walled Structures*, 75:103–112.
[28] Long, N. V., Loi, N. V., Binh, T. V. (2023). Vibration analysis of saturated functionally graded porous plates subjected to a moving load. *Journal of Science and Technology in Civil Engineering (STCE) - HUCE*, 17(4V):64–79.
[29] Long, N., Tu, T., Hung, D., Trung, D. (2024). Bending and buckling analysis of FGM nano plates with porosities based on non-local elasticity incorporating the surface effects. *Journal of Science and Technology in Civil Engineering (STCE) - HUCE*, 18(2V):140–156.
[30] Tung, H. V. (2016). Thermo-mechanical post-buckling of thick FGM plates resting on elastic foundations with tangential edge constraints. *Vietnam Journal of Mechanics*, 38(1):63–79.
[31] Do, D. T. T., Thai, S. (2023). Transient analysis of functionally graded plates using extreme gradient boosting. *Journal of Science and Technology in Civil Engineering (JSTCE) - HUCE*, 17(4):26–36.
[32] Hughes, T. J. R., Cottrell, J. A., Bazilevs, Y. (2005). Isogeometric analysis: CAD, finite elements, NURBS, exact geometry and mesh refinement. *Computer Methods in Applied Mechanics and Engineering*, 194(39):4135–4195.
[33] Cottrell, J. A., Hughes, T. J. R., Bazilevs, Y. (2009). *Isogeometric Analysis: Toward Integration of CAD and FEA*. 1st edition, Wiley Publishing.
[34] Reddy, J. N. (2000). Analysis of functionally graded plates. *International Journal for Numerical Methods in Engineering*, 47(1–3):663–684.
[35] Reddy, J. N. (1984). A Simple Higher-Order Theory for Laminated Composite Plates. *Journal of Applied Mechanics*, 51(4):745–752.
[36] Von Kármán, T. (1910). *Festigkeitsprobleme im maschinenbau*. Teubner.
[37] Reddy, J. N. (2004). *An Introduction to Nonlinear Finite Element Analysis*. Oxford University Press, New York.
[38] Wu, B., Pagani, A., Filippi, M., Chen, W. Q., Carrera, E. (2019). Large-deflection and post-buckling analyses of isotropic rectangular plates by Carrera Unified Formulation. *International Journal of Non-Linear Mechanics*, 116:18–31.
[39] Nguyen, V. P., Anitescu, C., Bordas, S. P. A., Rabczuk, T. (2015). Isogeometric analysis: An overview and computer implementation aspects. *Mathematics and Computers in Simulation*, 117:89–116.
[40] Crisfield, M. A. (1991). *Non-Linear Finite Element Analysis of Solids and Structures, Advanced Topics*. Wiley.
[41] Le-Manh, T., Lee, J. (2014). Postbuckling of laminated composite plates using NURBS-based isogeometric analysis. *Composite Structures*, 109:286–293.
[42] Sitli, Y., Mhada, K., Bourihane, O., Rhanim, H. (2021). Buckling and post-buckling analysis of a functionally graded material (FGM) plate by the Asymptotic Numerical Method. *Structures*, 31:1031–1040.